Carnegie Observatories Astrophysics Series, Vol. 3:
Clusters of Galaxies: Probes of Cosmological Structure and Galaxy Evolution, 2004
ed. J. S. Mulchaey, A. Dressler, and A. Oemler (Pasadena; Carnegie Observatories:
http://www.ociw.edu/ociw/symposia/series/symposium3/proceedings.html)

The Cluster Galaxy Circular Velocity Function

V. DESAI, J. J. DALCANTON, L. MAYER, D. REED, T. R. QUINN, and F. GOVERNATO
University of Washington, WA, USA

Abstract

We present galaxy circular velocity functions (GCVFs) for 34 low redshift ($z < 0.15$) clusters identified in the Sloan Digital Sky Survey Early Data Release (York et al. 2000; Stoughton et al. 2002; Smith et al. 2002; Gunn et al. 1998; Fukugita et al. 1996) for fifteen clusters drawn from dark matter simulations of hierarchical structure growth in a ΛCDM cosmology, and for ∼29,000 SDSS EDR field galaxies. We find that the observed and simulated cluster GCVFs take the form of a power law. The cumulative GCVFs of the simulated clusters are very similar across a wide range of cluster masses, provided individual subhalo circular velocities are scaled by the circular velocities of the parent cluster. Once all sources of error are accounted for, the intrinsic scatter in the cumulative, scaled observed cluster GCVF is consistent with the simulations. The slope of the observed cluster GCVF is ∼-2.5, independent of cluster velocity dispersion, $\sigma_{\rm cl}$. The average slope of the simulated GCVFs is somewhat steeper, although formally consistent given the errors. Using our highest resolution cluster, we find that the effects of baryons on galaxy rotation curves is to flatten the simulated cluster GCVF into better agreement with observations. Finally, we find that the field GCVF deviates significantly from a power law, being flatter than the cluster GCVF at circular velocities less than 200 km s^{-1}, and steeper at circular velocities greater than 200 km s^{-1}. Throughout we adopt $H_0 = 70 km\ s^{-1}{\rm Mpc}^{-1}$, $\Lambda = 0.7$, and $\Omega = 0.3$.

1.1 The Observed Cluster Galaxy Circular Velocity Function

For each cluster, galaxies within the virial radius and with $r^* < 21.5$ (Lupton et al. 2001) were classified as early or late type based upon their $u^* - r^*$ colors (Strateva et al. 2001). We calculated circular velocities ($V_{\rm c}$) for the late types using the inverse Tully Fisher Relation of Giovanelli et al. (1997). Line-of-sight velocity dispersions were calculated for early type galaxies using the inverse Fundamental Plane Relation, which we calculated from the distributions described in Bernardi et al (2003a,b,c). In order to plot early type galaxies on the same velocity scale as late types, we converted the line-of-sight velocity dispersion to $V_{\rm c}$ using the relation presented by Ferrarese (2002).

Shethet al. (2003) note that if the scatter in the mean inverse Tully Fisher and Fundamental Plane relations is significant, their use can significantly distort the shape of the GCVF. Therefore, in constructing our GCVFs, we accounted for the scatter by representing each galaxy's $V_{\rm c}$ as a probability distribution, rather than a single value.

Because a spectrum is not available for every galaxy in the field of each cluster, our background subtraction is statistical. We calculated V_c for every galaxy within the virial radius of each cluster under the assumption that it lies at the cluster redshift. Clearly, some galaxies have redshifts greater or less than that of the cluster, and our calculations were incorrect for these galaxies. This effect was removed during our background subtraction procedure. Again using the cluster redshift, we calculated V_c for every galaxy within an annulus bounded by inner and outer radii of 3 and 5 Mpc, respectively. These galaxies should have a redshift distribution similar to that of the cluster interlopers. Thus, by subtracting the appropriately normalized GCVF of galaxies in the annulus, we corrected for the interlopers.

1.2 Simulations

In order to compare our observational results against simulations, we compiled a set of 15 simulations of the dark matter components of clusters. Each simulated cluster was evolved in the currently favored ΛCDM cosmology with Λ=0.7, H_0 = 70 km $s^{-1} Mpc^{-1}$ Ω_0 = 0.3, and σ_8 = 1. Ten are the most massive clusters from the zero redshift output of the 50^3 h_{100}^{-3} Mpc^3 simulation described in Reed et al. (2003). An additional four clusters are described in Borgani et al. (2002).

The 14 cluster simulations were of sufficient resolution to robustly determine peak circular velocities in subhalos above the completeness velocities of our observed GCVFs. They were of insufficient resolution, however, to accurately trace subhalo internal density profiles. These were necessary to determine the effects of baryons on galaxy rotation curves (see §1.6). For this purpose, we used a very high resolution N–body simulation of a galaxy cluster with σ_{cl} = 600 km s^{-1} and $M_{vir} = 3 \times 10^{14} M_\odot$, represented by approximately one million particles within R_{vir} = 1.75 Mpc. It was evolved in a 100^3 Mpc^3 volume where the force spline softening was 1.25 kpc and the large scale structure was sampled at a lower resolution.

1.3 The Shape of the GCVF

In Figure 1.1 we plot the GCVFs for our sample of 34 clusters in three σ_{cl} bins. The power law form of the cluster GCVF is somewhat surprising. The cluster luminosity function is usually described by a Schechter function. Because the luminosities of both early and late type galaxies are related to their circular velocities by power laws ($L \propto V_c^n$), it is not obvious that the galaxy population as a whole should obey both a Schecter luminosity function and a power law GCVF.

In order to increase the signal to noise in in our determination of the cluster GCVF, we built composite cluster GCVFs using a technique analogous to that of Colless (1998) for building composite cluster luminosity functions. The composite cluster GCVFs in the three σ_{cl} bins are shown in the bottom panel of Figure 1.1. An increase in signal to noise still yielded a power law form.

1.4 Is Cluster Substructure Self-Similar?

Moore et al. (1999) found that the cumulative GCVF for a Virgo-like simulation is identical to that of subhalos within a Milky-Way-like simulation, provided the velocities are scaled by the velocity of the parent halo (V_{cl}). In the top panel of Figure 1.2, we have plotted the cumulative, scaled GCVF for all fifteen simulated clusters. Our simulated clusters have very similar cumulative, scaled GCVFs, in agreement with the results of Moore et al. (1999).

In the bottom panel of Figure 1.2, we plot the same quantity for our sample of SDSS

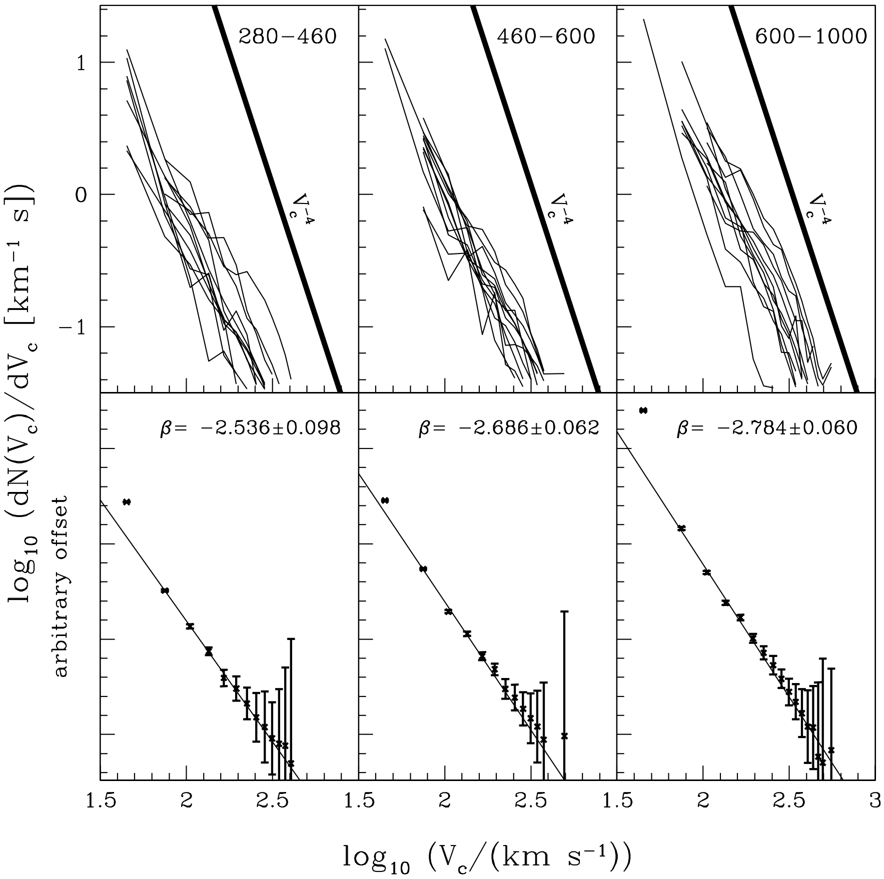

Fig. 1.1. The observed CGVFs, binned by $\sigma_{\rm cl}$. *Top panels:* Individual cluster GCVFs are shown with thin lines. The bold lines have a slope of -4, motivated by a Press-Schechter mass function and by simulations (Moore et al. 1999; Ghigna et al. 2000), and are for reference only. Ranges of $\sigma_{\rm cl}$ are shown in the upper right of each panel, in km s^{-1}. *Bottom panels:* Each panel shows the composite GCVFs constructed from clusters having $\sigma_{\rm cl}$ in the range indicated in the panel directly above. Error bars take into account Poisson error in counting galaxies both within $R_{\rm vir}$ and in the background annulus. We overplot the best-fit power laws, and indicate their slopes in the upper right hand corner of each panel.

clusters. The slopes and offsets of the simulated and observed clusters cannot be compared directly, since the effects of baryons have not been included in the simulations. However, assuming that baryonic physics changes the shapes of all the GCVFs in a similar way, we can compare the scatter in the observed and simulated GCVFs. We found that, once the measurement errors in $\sigma_{\rm cl}$ and the scatter due to Poisson noise were accounted for in the observations, they show the same degree of variation found in ΛCDM dark matter cluster simulations.

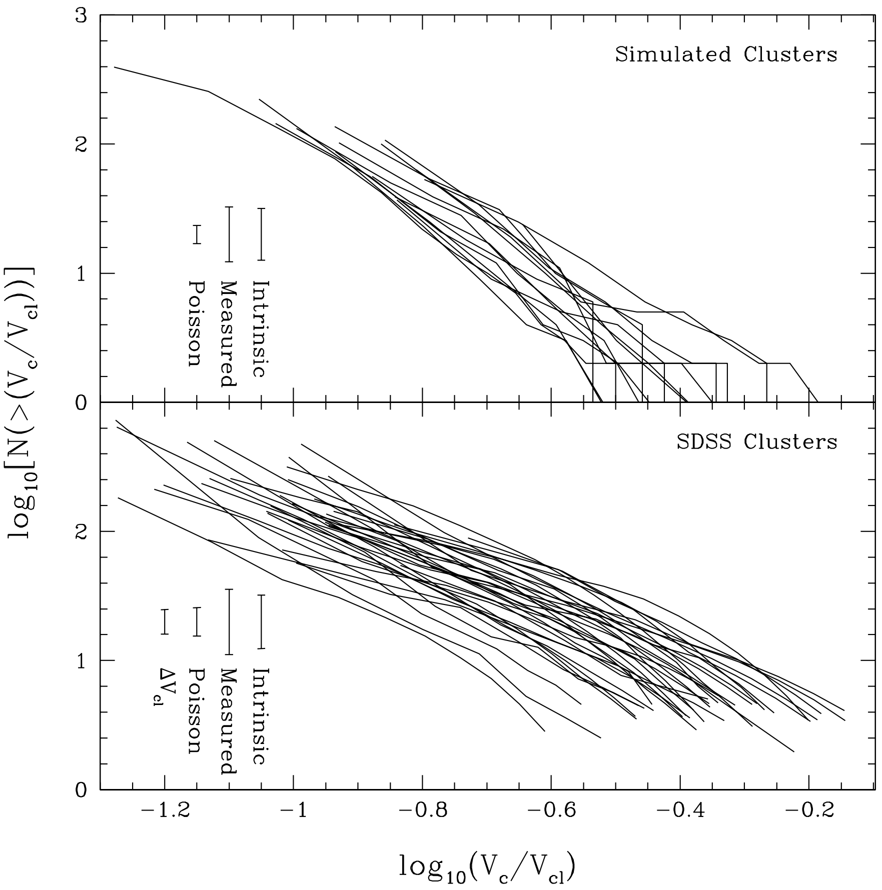

Fig. 1.2. The simulated and observed CGVFs, with galaxy circular velocities scaled by cluster circular velocites. The error bars have length 2Δ, where Δ is the RMS scatter at $\log_{10}(V_c/V_{cl} \approx -0.7)$ due to various sources, as labelled. *Poisson* refers to Poisson noise in counting galaxies within R_{vir} for the simulated clusters and to Poisson noise in counting galaxies within R_{vir} and the background annulus for the SDSS clusters. *Measured* refers to the total measured scatter. ΔV_{cl} refers to the scatter in $\log_{10}[N(>(V_c/V_{cl}))]$ due to errors in measuring V_{cl}, and *Intrinsic* refers to the portion of the total measured scatter unaccounted for by Poisson scatter in the case of the simulations or by both Poisson scatter and that induced by ΔV_{cl} for the SDSS clusters.

1.5 Trends in the Cluster GCVF with Cluster Velocity Dispersion

The observed and simulated cluster GCVFs are well-fit by a power law. The top panel of Figure 1.3 shows that the slope does not vary systematically with σ_{cl} for either the observed or the simulated clusters. The mean slope for the simulated GCVFs is $\overline{\beta_{sim}} = -3.4 \pm 0.8$, which is somewhat steeper than the mean for the observations, $\overline{\beta} = -2.5 \pm 0.8$, although they are formally consistent. It should be noted that the slopes are not directly comparable because the simulations do not account for the effects of baryons.

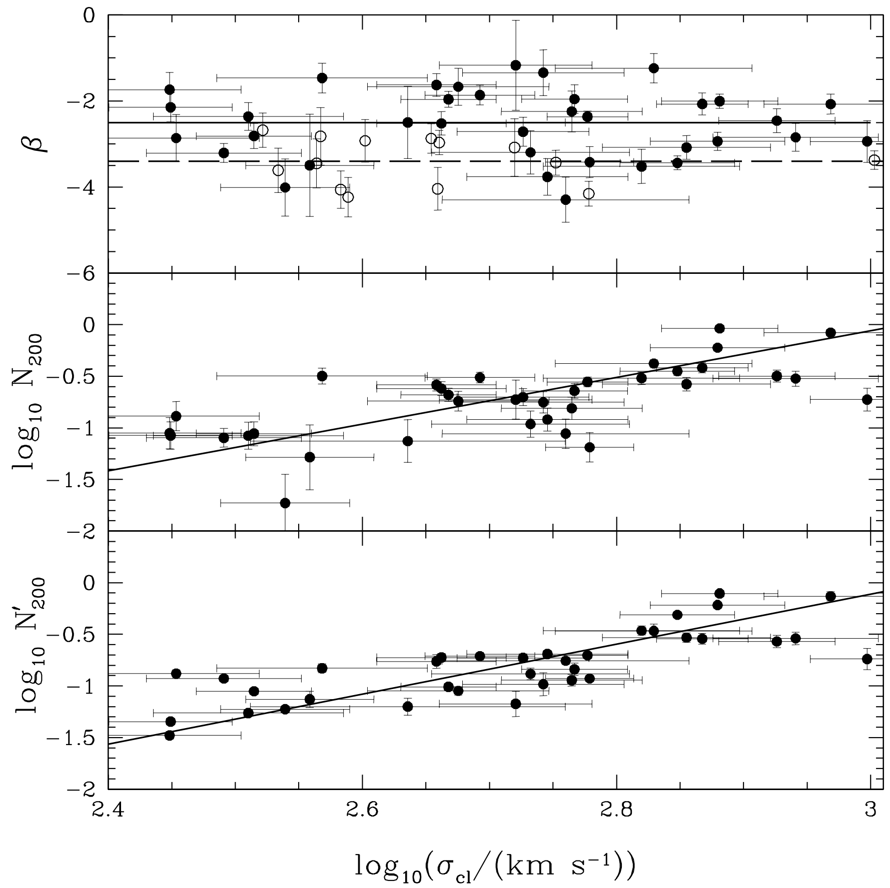

Fig. 1.3. Each observed and simulated cluster GCVF was fit to the equation $\log_{10}(dN/dV_c) = \log_{10} N_{200} + \beta \log_{10}\left(V_c/200 \text{ km s}^{-1}\right)$. *Top Panel:* The slope of the cluster GCVF as a function of σ_{cl}. Solid points are for the observed cluster GCVFs, which have a mean value of $\overline{\beta} = -2.5 \pm 0.8$ indicated by the solid line. Open points are for the simulated cluster GCVFs, which have a mean value of $\overline{\beta_{sim}} = -3.4 \pm 0.8$ indicated by a dashed line. *Middle Panel:* The normalization of the observed cluster GCVF as a function of σ_{cl}. High σ_{cl} clusters tend to contain more galaxies than low σ_{cl}. The line that best fits this trend is given by $\log_{10} N_{200} = (2.26 \pm 0.2)\log_{10}\sigma_{cl} - (6.84 \pm 0.6)$ and is overplotted. *Bottom Panel:* The normalizations of the fits for the observed cluster GCVFs were recomputed while holding the slope fixed to the mean value shown in the top panel. The new normalizations are plotted against σ_{cl} in the bottom panel. The line that best fits these data is $\log_{10} N'_{200} = (2.42 \pm 0.2)\sigma_{cl} - (7.37 \pm 0.5)$ and is overplotted.

The normalizations of the observed cluster GCVFs are plotted in the middle panel of Figure 1.3 and show a clear systematic trend in the sense that higher mass clusters host more galaxies. We recalculated the normalizations with the slope fixed to its mean value of −2.5. These values are plotted against σ_{cl} in the third panel of Figure 1.3.

1.6 The Effects of Baryons on the Cluster GCVF

A more meaningful comparison between observations and simulations would require a determination of the circular velocity profile taking into account the effects of both dark matter *and* baryons. Baryons affect the circular velocity profile of a galaxy in two ways. First, they significantly contribute to the enclosed mass at small radii. Second, they adiabatically pull the dark matter into a more concentrated equilibrium configuration than it would have in their absence. The degree of these effects depends on the mass distribution of the baryons. We populated the subhalos with galaxies in a way that mimics, as closely as possible, observed empirical relations.

In Figure 1.4, we compare the GCVF measured in our highest resolution simulation to that of the SDSS clusters that have similar values of $\sigma_{\rm cl}$. The simulated cluster GCVF uncorrected for baryons is too steep, underpredicting the number of galaxies at high $V_{\rm c}$. When the effects of baryons were included, the number of high $V_{\rm c}$ galaxies increased, while the number of low $V_{\rm c}$ galaxies decreased, bringing the simulations into better agreement with the observations.

1.7 The Cluster Versus Field GCVF

To allow a direct comparison to our cluster GCVFs, we constructed a field GCVF using the same relations that we used in the previous cluster analysis. We selected galaxies from the SDSS EDR spectroscopic sample with $14.5 < r^* < 17.77$. Each of the resulting $\sim$29,000 galaxies was assigned a weight equal to the inverse of the volume over which the galaxy could be observed, given the apparent magnitude limits. The cluster GCVF shows much less curvature than that of the field, being steeper for $V_{\rm c} < 200$ km s^{-1} and more shallow for $V_{\rm c} > 200$ km s^{-1}, as illustrated in Figure 1.5.

1.8 Acknowledgments

VD and DR acknowledge funding from the Graduate Student Researchers Program, JJD was partially supported through the Alfred P. Sloan Foundation, and TRQ was partially supported by the National Science Foundation.

Funding for the creation and distribution of the SDSS Archive has been provided by the Alfred P. Sloan Foundation, the Participating Institutions, the National Aeronautics and Space Administration, the National Science Foundation, the U.S. Department of Energy, the Japanese Monbukagakusho, and the Max Planck Society. The SDSS Web site is `http://www.sdss.org/`.

The SDSS is managed by the Astrophysical Research Consortium (ARC) for the Participating Institutions. The Participating Institutions are The University of Chicago, Fermilab, the Institute for Advanced Study, the Japan Participation Group, The Johns Hopkins University, Los Alamos National Laboratory, the Max-Planck-Institute for Astronomy (MPIA), the Max-Planck-Institute for Astrophysics (MPA), New Mexico State University, University of Pittsburgh, Princeton University, the United States Naval Observatory, and the University of Washington.

References

Bernardi M., et al. 2003, AJ, 125, 1817
Bernardi M., et al. 2003, AJ, 125, 1849
Bernardi M., et al 2003, AJ, 125, 1866
Borgani, S. 2002, MNRAS, 336, 409
Colless M., 1989, MNRAS, 237, 799
Ferrarese, L., 2002, ApJ, 578, 90

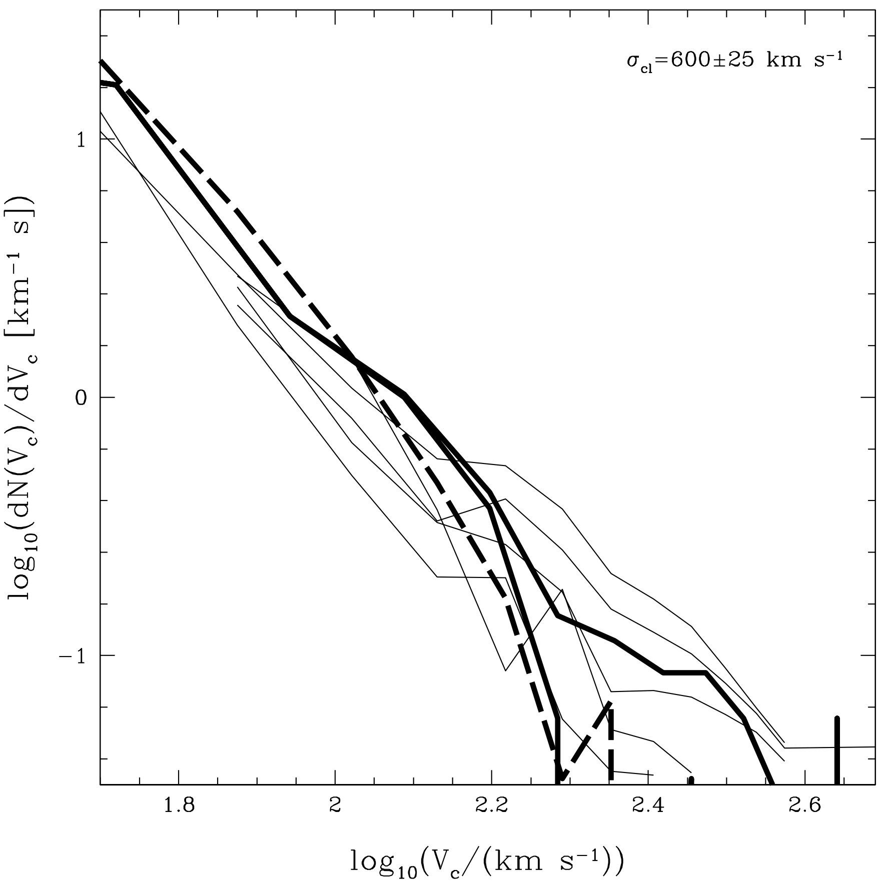

Fig. 1.4. Comparison of the GCVF measured from our highest resolution galaxy cluster simulation to that measured in SDSS clusters. The dashed line is the simulated GCVF constructed using peak circular velocities. The bold lines bracket simulated GCVFs which have been corrected for the effects of baryonic infall. We varied the total mass that infalls to form ellipticals and the peak circular velocity above which subhalos host early type rather than late type galaxies. Thin lines are the GCVFs measured in SDSS clusters with σ_{cl} within 25 km s^{-1} of that measured for the simulated cluster.

Fukugita, M., Ichikawa, T., Gunn, J. E., Doi, M., Shimasaku, K., Schneider, D. P. 1996, AJ, 111, 1748

Ghigna, S., Moore, B., Governato, F., Lake, G., Quinn, T., & Stadel, J. 2000, ApJ, 544, 616

Giovanelli, R., Haynes, M. P., Herter, T., Vogt, N. P., da Costa, L. N., Freudling, W., Salzer, J. J., Wegner, G. 1997, AJ, 113, 53

Gonzalez, A. H., Williams, K. A., Bullock, J. S., Kolatt, T. S., & Primack, J. R. 2000, ApJ, 528, 145

Gunn, J. E. et al. 1998, AJ, 116, 3040

Lupton, R. H., Gunn, J. E., Ivezić, Z., Knapp, G. R., Kent, S., Yasuda, N. 2001, in ASP Conf. Ser. 238: Astronomical Data Analysis Software and Systems X Vol. 10, The SDSS Imaging Pipelines, p. 269

Moore, B., Ghigna, S., Governato, F., Lake, G., Quinn, T., Stadel, J., Tozzi, P. 1999, ApJL, 524, L19

Reed, D., Gardner, J., Quinn, T., Stadel J., Fardal, M., Lake, G., & Governato, F. 2003, MNRAS, 346, 565

Sheth, R. K. et al. 2003, MNRAS, 345, 62

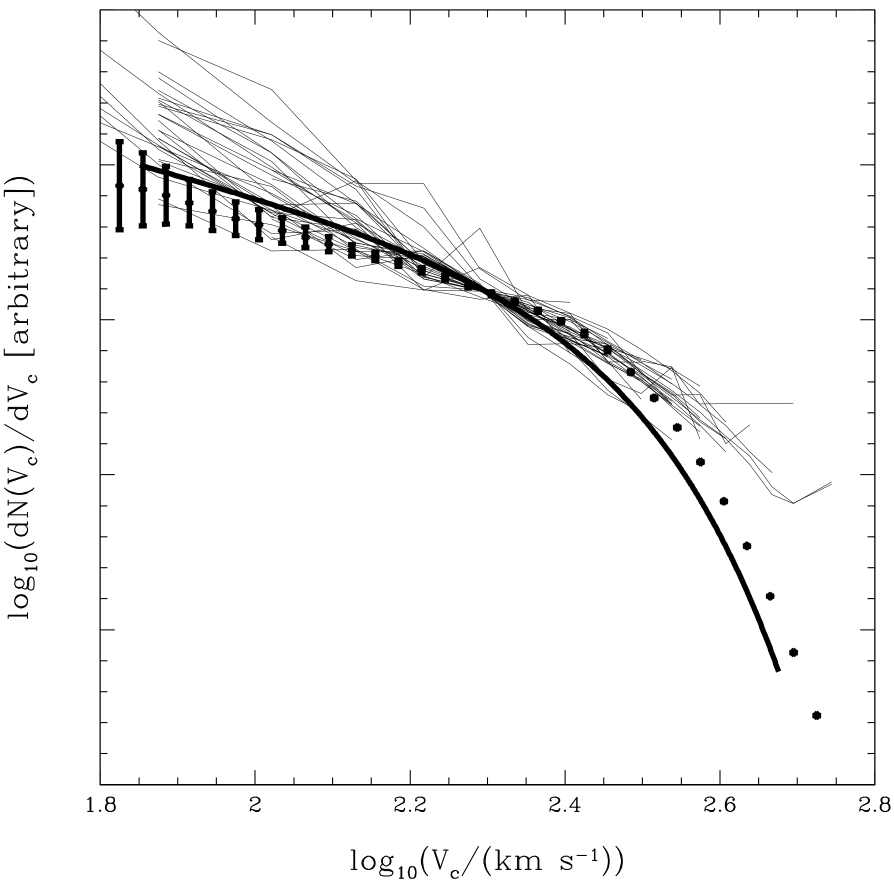

Fig. 1.5. GCVFs for the SDSS cluster sample and the field. The points with error bars represent the field GCVF determined from SDSS data, normalized at $\log_{10}(V_c/\mathrm{km\ s^{-1}}) \approx 2.3$. The solid bold line is the similarly normalized observed field GCVF as determined by Gonzalez et al. (2000). Because of the arbitrary normalization, this plot is suitable only for assessing differences in the shape of the GCVF in clusters and the field.

Smith, J. A. et al. 2002, AJ, 123, 2121
Stoughton, C. et al., 2002, AJ, 123, 485
Strateva, I. et al., 2001, AJ, 122, 1861
York, D. G. et al., 2000, AJ, 120, 1579